The Sun as an X–ray Star I: Deriving the Emission Measure Distribution vs. Temperature of the Whole Solar Corona from the Yohkoh/SXT Data

S. Orlando[1,2], G. Peres[2], and F. Reale[2]

[1]Solar System Division, ESA Space Science Dept., ESTEC, Postbus 299, NL–2200 AG Noordwijk, The Netherlands

[2]Dip. di Scienze Fisiche ed Astronomiche – Sez. di Astronomia – Univ. di Palermo, Piazza del Parlamento 1, I–90134 Palermo, Italy

ABSTRACT

The scope of this work is to obtain the emission measure distributions vs. temperature, EM(T), of the whole solar corona from Yohkoh/SXT images. As discussed in Paper II, the EM(T) is our starting point to study the Sun as an X–ray star. To this purpose, we need to extract as much information as possible from the Yohkoh/SXT data covering the whole range of the Yohkoh/SXT temperature sensitivity, i.e. $5.5 < \log T(\mathrm{K}) < 8$. In particular at low photon counts and temperatures below 10^6 K errors on the temperature and emission measure determination are expected to be large. To this end we have made an extensive set of simulations to explore the nominal performance of the entire system (instrument and data analysis system) in the determination of the plasma temperature and emission measure at low, intermediate and high photon counts per pixel. We have shown that low–count data with a number of photons per pixel $n_{\mathrm{phot}} < 10$ are affected by large errors and lead to the derivation of an unrealistic EM(T) characterized by a steep negative slope. As a result, we have devised an analysis method which minimizes the instrumental and statistical effects on the determination of EM(T) and allows us to determine the global coronal EM(T). As a first application to real SXT data, we have derived the EM(T) of the Sun close to the maximum of the solar cycle, a challenging case. The low temperature part is in agreement with analogous studies made in the UV band and it shows a well defined maximum at $T \sim 2$ MK.

Subject headings: Sun: activity, Sun: corona, stars: activity, stars: coronae

1. Introduction

The Yohkoh Soft X–ray Telescope (SXT) has been collecting a very large number of X–ray images of the Sun since 1991, allowing us to study the corona morphology, its evolution as well as the plasma's temperature, T, and emission measure, EM, of the coronal structures over more than one half of a solar cycle.

The SXT typically monitors the whole solar corona and at the same time allows us to resolve in detail the coronal structures, and to follow their evolution. The SXT data are, therefore, an ideal template to interpret spatially unresolved stellar coronal data. As we discuss here and in Paper II (Peres et al. 1999), such data can be used to derive a description of the corona as a whole entity and to understand the contributions of the various structures and regions to the solar overall X–ray emission.

Our project, in general, is to employ such data to bridge the gap between solar and stellar coronal physics and, to some extent, to apply the insight of solar physics to stellar physics (and vice–versa), as discussed in Paper II. The first, and fundamental, step of this project is to derive the distribution of the emission measure vs. the line–of–sight averaged temperature, EM(T), of the whole corona from SXT observations. EM(T) provides by itself important insight into the physics of the whole corona. Then, from the EM(T), by means of a spectral synthesis code, we synthesize the X–ray spectrum of the whole solar corona. Finally, by folding the spectrum with the response of non–solar instruments, for instance Rosat/PSPC (i.e. the Position Sensitive Proportional Counter on board the Roentgen Satellit) or ASCA/SIS (i.e. the Solid–state Imaging Spectrometer on board the Advanced Satellite for Cosmology and Astrophysics), we synthesize an observation of the Sun with such instruments, as if it were a star: thus we can compare directly solar and stellar X–ray observations.

Deriving temperature and emission measure from images taken through two different filters, a crucial step in our work, is a standard procedure of Yohkoh data analysis and has been extensively applied to study the physical characteristics of coronal structures observed with the SXT (e.g. Tsuneta 1992, Kano & Tsuneta 1995). However most of such studies typically consider only high signal–to–noise SXT data and pertain to temperatures over a limited part of the whole temperature SXT sensitivity range, typically where the response is better.

Instead, our task requires to derive the emission measure distribution of the whole corona simultaneously and in the whole range of SXT temperature sensitivity. In particular, it is important to obtain reliable EM values at temperatures below 1 MK, a range of temperatures over which many non–solar X–ray telescopes, e.g. Rosat, XMM (the X–ray Multi–Mirror Mission), have high sensitivity. Even in the softest filters, routinely used for full–disk SXT observations, such temperatures are in the part of the filter response where the filter sensitivity is very low. Therefore, in typical observations, even large amounts of plasma at low temperatures are detected by the SXT at low signal to noise ratio (i.e. large statistical uncertainty), leading to large uncertainties in the temperature value and, given the steep curve of the SXT signal vs. temperature, to even larger errors in the emission measure values. As a result, if our analysis were to include all pixels of the SXT full disk images without any kind of screening, one would invariably obtain an emission measure distribution with large errors. Indeed in this case we have typically found very high and unrealistic values below 10^6 K and different from the results obtained by other studies, e.g. those recently made in UV by Brosius et al. (1996) and by Landi & Landini (1997). The SXT has been optimized to study plasma at temperatures of a few 10^6 K rather than below 10^6 K. In order to derive the EM(T) distribution of the whole Sun in the full temperature range $10^{5.5}$ K $< T < 10^8$ K, a significant part of our effort has been to include in our analysis also the pixels at low temperatures, i.e. outside the SXT optimal range, and therefore to extract as much information as possible from the SXT data.

Indeed a large part of the difficulties in deriving the complete EM(T) from the SXT images originates from the wide dynamic range of the corona X–ray brightness. Although fast sequences of images of different exposure times help to sample better both bright and faint regions of the corona, only rarely the exposure times in a sequence have been selected so as to have an adequate signal to noise ratio over the whole corona, after combining the information from the various images. A careful treatment of low signal–to–noise regions is therefore needed anyway.

This paper illustrates our method to extract a correct distribution of the emission measure vs. temperature of the whole solar corona from the available sequences of SXT images, including pixels at low and high statistics, simultaneously and over the $10^{5.5} - 10^8$ K nominal temperature range of SXT. We take particular care of the regimes of low photon counts and of the extremes of the temperature ranges, where the errors in T and EM can be large (Kano & Tsuneta 1995, Yoshida et al. 1995, Yoshida & Tsuneta 1996, Tsuneta 1996, Brosius et al. 1997).

In order to devise a criterion to discriminate reliable from unreliable data in any photon count regime, we make a large set of simulations of SXT detections of isothermal plasmas, over the entire range of temperatures and of photon count statistics accessible with the SXT.

The uncertainties in the determination of temperature and emission measure with SXT have already been the subject of a study by Klimchuk & Gary (1995). Acton (1997) presented additional analysis of the SXT temperature determination vs. plasma temperature. Our simulations may help to clarify further the issue of error analysis of SXT data at low photon counts.

Porter & Klimchuk (1995) have also made extensive use of simulations to understand the Yohkoh/SXT performance, concentrating, however, on high photon counts and on cases with temperature in the few 10^6 K range (i.e. where Yohkoh/SXT soft filters work better). Our study is instead dedicated to the whole nominal Yohkoh/SXT temperature range and to all photon count values of interest in observations, and has a rather different focus.

Watanabe et al. (1995) derived the EM(T) limitedly to active regions and showed the presence of plasma at several millions degrees. That analysis was concentrated on active regions while we study the whole solar corona (in order to compare the Sun with other stars).

The paper is structured as follows: in section 2 we describe the SXT data simulations and their analysis; in section 3 we analyze real SXT data and describe the screening criterion; and in section 4 we discuss our results and draw our conclusions.

2. Yohkoh/SXT data simulations

Yohkoh/SXT is a grazing incidence telescope capable of imaging solar plasma emission in the $1.27 - 70$ Å nominal wavelength range (Tsuneta et al. 1991); it forms X–ray wide–band photometric images on a CCD detector, each pixel giving a digital CCD output called Data Number (in the following DN). SXT can discriminate different X–ray bands with six broad filters to provide a pixel–by–pixel plasma temperature diagnostic. The physical analysis of the SXT measurements is carried out under the isothermal plasma approximation: it derives the line of sight average isothermal temperature and emission measure in each pixel over the solar disk and it does not include variations in T and EM within the field of view of a single pixel. Specifically, the temperature of the plasma imaged in each pixel is obtained from the ratio between fluxes, measured with two different filters, using appropriate conversion factor curves derived from the instrumental response and spectral models (the so–called *filter ratio method*, Vaiana, Krieger, & Timothy 1973, Gerassimenko & Nolte 1978, Hara et al. 1992). The emission measure is, then, derived from the flux measured through one of the two filters, by using the estimated temperature.

The scope of this work is to explore in detail the nominal performance of the instrument and of the Standard Yohkoh Analysis System (SYAS) in the process of temperature and emission measure determination, from low to high photon counts (and therefore from low to high signal to noise ratio in the pixel) and from low to high temperatures, within the nominal $10^{5.5}$ – 10^8 K instrument sensitivity range. We will thus find out which pixels are unreliable and ought to be discarded. To this end we simulate the detection of the plasma emission in a single pixel and in the instrument spectral bands of interest. Then, we analyze the response of a single pixel for the possible conditions we expect to find in an image. More in detail, our simulations can be sketched as in Fig. 1: choosing the temperature and emission measure values of the plasma imaged in the pixel; synthesis of the X–ray spectrum emitted by the plasma[1]; folding the spectrum through the instrumental response which SXT has with two different filters; fixing the number of photons detected in both filter bands; generating a large set of different simulations of the SXT data number in the pixel for each of the two bands; deriving with SYAS the temperatures and emission measures of the simulated data; studying how they are distributed around the input parent values. We repeat this process for a range of photon counts values, and sampling uniformly the whole SXT temperature range $10^{5.5} - 10^8$ K. This method also provides us with a detailed insight of the errors simultaneously present in various parts of full disk SXT images.

We also study how a "parent" distribution of emission measure vs. temperature can be affected by errors for different photon count statistics, looking for possible systematic effect and, more in general, effects on the global EM(T).

---

[1]We have consistently used the MEKAL spectral model in every step of our analysis: the synthesis of the simulated X–ray spectra, the determination of the filter response and of the filter ratio vs. plasma temperature used to derive the temperature and emission measure in the SYAS. The MEKAL model has been used because it is more up to date than the Mewe, Gronenschild, & van den Oord (1985) model (adopted for SYAS) and is largely used in astrophysics.

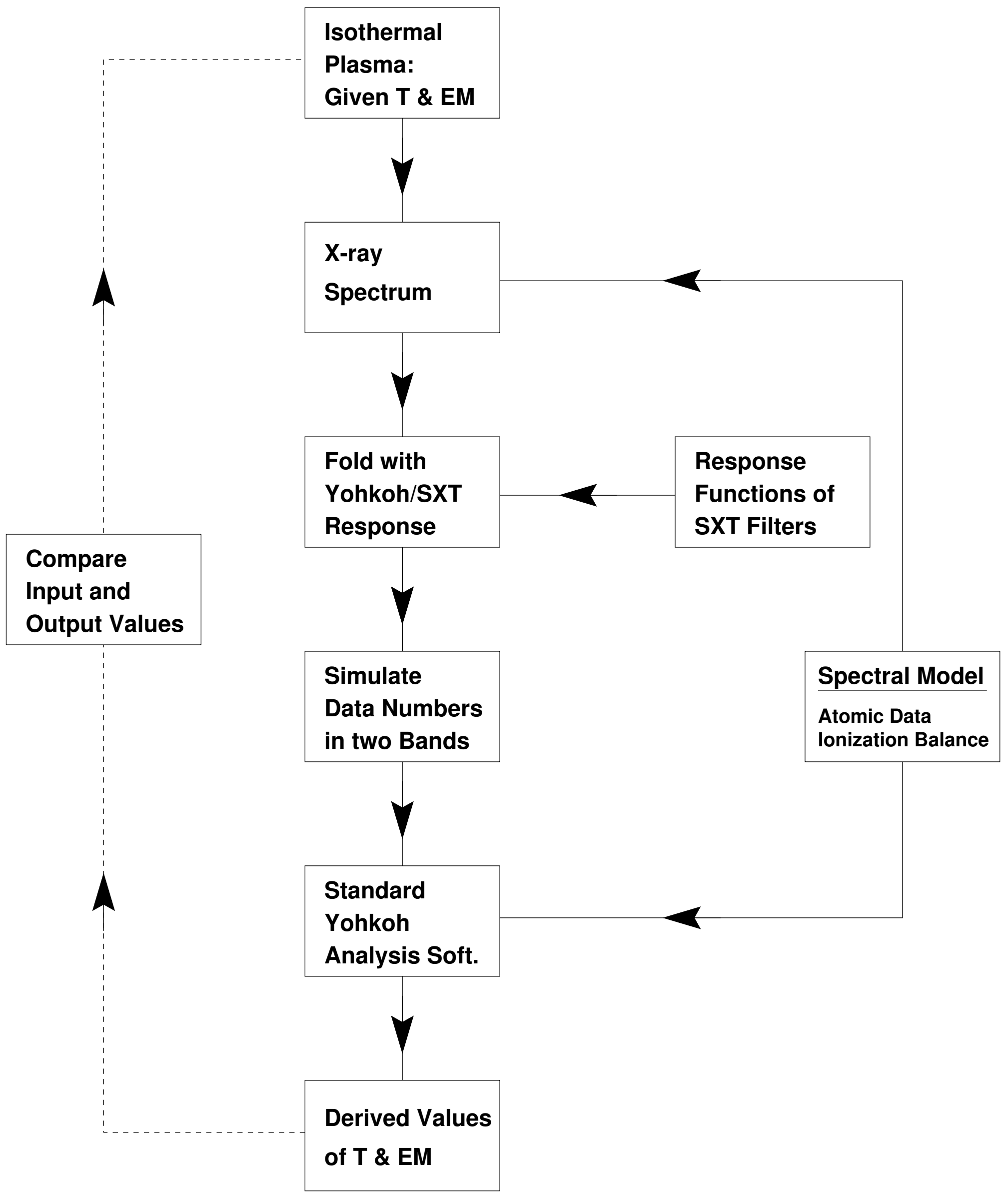

Fig. 1.— Scheme of our simulations of the Yohkoh/SXT data: we consider isothermal plasma with a prescribed value of temperature and emission measure; we then synthesize the relevant emitted spectrum using the MEKAL spectral code and convolve it with the response functions of SXT in the various bands. We then derive the number of electrons produced in the CCD and the output Data Numbers, obtaining a simulation of SXT data. We apply the SYAS to the simulated data to derive the "measured" temperature and emission measure and, finally, we compare them to the input ones.

2.1. Description of the simulations

For a given pair of values of input plasma temperature and emission measure, we synthesize the X–ray spectrum in the instrument wavelength band, including the whole SXT nominal bandwidth

$$N_\gamma(i,T) = \mathrm{EM} \int dE \; P(T,E)/E \qquad (1)$$

where $N_\gamma(i,T)$ is the number of photons in the wavelength bin i, EM is the emission measure, E is the photon energy, $P(T,E)$ is the spectrum emitted by an optically thin isothermal plasma, and the integral is computed over the energy range relevant for the i–th bin. The emitted spectrum is computed with the MEKAL spectral model (Kaastra 1992; Mewe, Kaastra, & Liedhal 1995) in 4000 wavelength bins.

Then we convolve the synthetic spectrum $N_\gamma(i,T)$ with the instrumental response functions of SXT in the bands typically used for full disk observations outside flares, namely the thin aluminum (Al 1265 Å, referred to as Al.1) and Al/Mg sandwich (comprising Al 2930 Å, Mg 2070 Å, Mn 562 Å, and C 190 Å, referred to as AlMg) filters. We obtain, for each input pair of values (T, EM), the filtered photon counts per wavelength bin in the focal plane,

$$N_{\gamma f}(i,T) = \frac{t_{\mathrm{exp}}}{4\pi D^2} N_\gamma(i,T) A_{\mathrm{eff}}(i) \;, \qquad (i = 1, ..., k) \qquad (2)$$

where i is the label of the wavelength bins, k is the total number of wavelength bins, $D(= 1$ AU) is the distance to the Sun, t_{exp} is the exposure time, and $A_{\mathrm{eff}}(i)$ is the filter effective area[2] in that band for the i–th wavelength bin.

The scope of our simulations include to evaluate how our results depend on the photon counts (i.e. the signal to noise ratio). To this end, we prescribe the exposure time so as to fix the total number of detected photons $n_{\mathrm{phot}} = \sum_{i=1}^{k} N_{\gamma f}(i,T)$, i.e. the photon counts summed over all the wavelength bins.

For instance, collecting 100 photons from a plasma with an EM $= 10^{47}$ cm^{-3} in the band of the Al.1 filter will require an exposure time of $t_{\mathrm{exp}} = 10.05$ s if $\log T = 5.6$, $t_{\mathrm{exp}} = 5.12 \times 10^{-3}$ s if $\log T = 6.3$ and $t_{\mathrm{exp}} = 7.3 \times 10^{-4}$ s if $\log T = 7$; for the same plasma, in the AlMg band, instead collecting 100 photons will require an exposure time of $t_{\mathrm{exp}} = 89.8$ s if $\log T = 5.6$, $t_{\mathrm{exp}} = 1.16 \times 10^{-2}$ s if $\log T = 6.3$ and $t_{\mathrm{exp}} = 1.16 \times 10^{-3}$ s if $\log T = 7$.

---

[2]The factors that determine the SXT filter effective area are: the double entrance filter transmission, the mirror reflectivity including the obscuration from the support structures, the analysis filter transmission, and the CCD quantum efficiency (Tsuneta et al. 1991). The number of electrons generated by a photon (actually another probability function) which is a fundamental feature of the CCD response is also taken into account in Eq. 3.

For realistic simulations, we account for statistical noise in the photon spectrum: we randomize the photon count $N_{\gamma f}(i,T)$ of the folded spectrum defined by Eq. 2 within each wavelength bin according to Poisson statistics. To this purpose, we used the *rejection method* applied to the Poisson distribution (Press et al. 1986). Note that, two realizations with the same input pair of values (T, EM) are different due to the Poisson randomization.

The number of photons detected by the CCD in each wavelength bin is then converted to the corresponding number of electrons produced in the CCD:

$$N_e = \frac{1}{3.65} \sum_{i=1}^{k} h\nu_i N_{\gamma f}(i,T) \tag{3}$$

where $h\nu_i$ is the average photon energy in eV in the wavelength bin i, and 3.65 eV$/e^-$ is the average energy required to produce one electron–hole pair in the silicon. Finally the digital CCD output, i.e. the data number DN, is (Tsuneta et al. 1991):

$$\mathrm{DN} = N_e/G(e^-/\mathrm{DN}) \tag{4}$$

where $G(e^-/\mathrm{DN})$ is the CCD camera gain constant which we assumed equal to 100 e^-/DN, i.e. the standard value defined prior to launch (Morrison 1994).

From the DN values obtained for the two selected filters, we derive the temperature and the emission measure as from real data, by using SYAS. We can then compare the result to the input value and proceed to further analysis.

2.2. Results of the simulations

One of the test we have made evaluates how an input EM(T) distribution with the same emission measure at all temperatures will emerge after all the effects of the observations and the data analysis. More specifically, as starting condition for our simulations, we assume as input distribution of emission measure vs. temperature $\mathrm{EM}_{in}(T_{in}) = 10^{47}$ cm^{-3} for $10^{5.5}$ K $\leq T_{in} \leq 10^8$ K.

The distribution is sampled at 24 values of input temperature T_{in} spaced uniformly in $\log T$ and the function we used is

$$\mathrm{EM}_{in}(T_{in}) = 10^{47} \times \delta(T_{in}) \quad \mathrm{cm}^{-3} \qquad (10^{5.5}\ \mathrm{K} \leq T_{in} \leq 10^8\ \mathrm{K}) \tag{5}$$

where $\delta(T_{in})$ is the normalized Dirac function. We simulate four values of the total number of photons in the SXT band, $n_{\rm phot} = 10, 10^2, 10^3, 10^4$; $n_{\rm phot}$ is the same in both SXT bands. The maximum count statistics ($n_{\rm phot} = 10^4$) has been selected to take into account that a CCD pixel can collect up to 3×10^5 electrons before saturation (Tsuneta et al. 1991).

For each seed temperature T_{in} and count statistics n_{phot}, we performe 10^4 realizations (i.e. simulations randomized differently according to the Poisson statistics) of each pair of photon spectra folded through the two SXT filter responses. For each realization, we derive the temperature T_{out} and the emission measure EM_{out} with the SYAS from the flux ratio in the pixel[3].

Finally we study the distribution of T_{out} and EM_{out} output values for each pair input values T_{in} and EM_{in}. Figs. 2, 3 and 4, show a selection of the results for different values of T_{in} and for $n_{\rm phot} = 10$, 10^2 and 10^4 in each spectral band.

At the lowest count statistics ($n_{\rm phot} = 10$; Fig. 2), the distributions of T_{out} and EM_{out} are highly non–Gaussian, and they have different characteristics in two ranges of temperatures T_{in}: for $\log T_{in}(\mathrm{K}) < 7$, T_{out} values appear dispersed and approximately centered around T_{in} (Fig. 2a); for $\log T_{in}(\mathrm{K}) \gtrsim 7$, T_{out} systematically underestimates T_{in} and, in particular, invariably $\log T_{out}(\mathrm{K}) \sim 7$. The SXT filter signal ratio vs. temperature is rather insensitive to variations for $\log T_{in}(\mathrm{K}) \gtrsim 7$, and, as a consequence, the temperature in this range and with the pair of filters used, namely Al.1 and AlMg, is ill determined (see Fig. 5, to be compared with the analogous figures in the *Yohkoh data analysis manual* (Morrison 1994) which are an updated version of the analogous ones in Tsuneta et al. (1991)). The curves in Fig. 5 have been derived using the nominal Yohkoh/SXT spectral response in the various bands and the updated MEKAL code.

Temperature diagnostics for $T \gtrsim 10^7$ K is possible with other SXT filters ratios, in particular Al 11.6 μm (referred to as Al12) and Be 119 μm (Be119) filters (see Fig. 5), which however are used mainly when the instrument is in the "flare–mode".

If $n_{\rm phot}$ increases, for $\log T(\mathrm{K}) < 7$, T_{out} values are less dispersed; the systematic underestimate of temperatures for $\log T(\mathrm{K}) > 7$ is also progressively reduced (Figs. 3 and 4). The influence of the higher signal to noise ratio is even more evident on the EM_{out} distributions: while for low photon counts the emission measure can be undetermined by orders of magnitude, for $n_{\rm phot} = 100$, the indetermination is reduced to less than one order of magnitude (see Fig. 3).

It is worth noting that a significant factor contributing to the deviation of the non–Gaussian asymmetric shape of the profiles is due to how the flux ratio varies with solar temperature (Tsuneta 1991, Klimchuk & Gary 1995).

Fig. 6 shows the T_{out} and EM_{out} median values and their 68% and 90% confidence ranges (corresponding to ± 1 and $\pm 1.6\ \sigma$ in the case of a Gaussian distribution). When the count statistics is low ($n_{\rm phot} = 10$) the temperature and the emission measure are intrinsically ill–determined for any T.

---

[3]We cannot compute the temperature for the realizations which yield a filter ratio outside the range of permitted values.

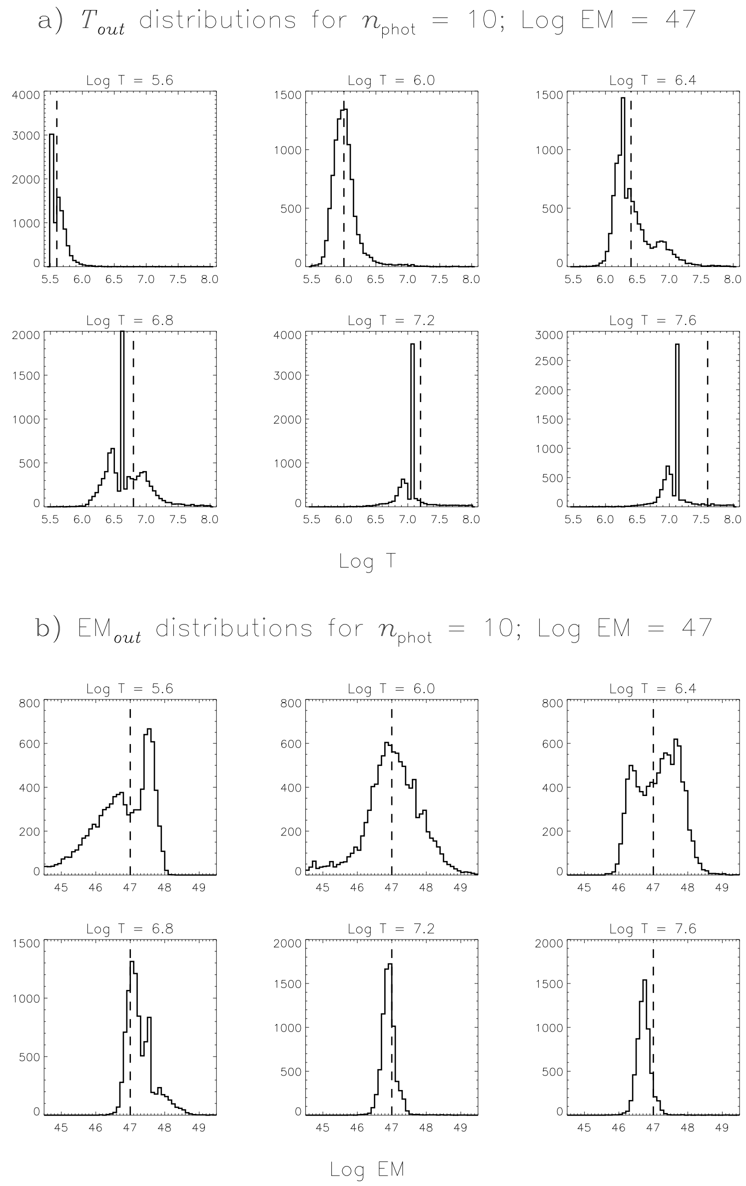

Fig. 2.— Distributions of T_{out} (panel a) and the relevant EM_{out} (panel b) as derived from the flux ratios simulated for various pairs of input values $(T_{in}, \mathrm{EM}_{in})$. Here we show 10^4 realizations for each pair $(T_{in}, \mathrm{EM}_{in})$. The number of collected photons is $n_{\rm phot} = 10$ in each band, and $\mathrm{EM}_{in}(T_{in}) = 10^{47}$ cm^{-3} (see Eq. 5). The vertical dashed lines mark the position of the "parent" values T_{in} and EM_{in}. The relevant value of T_{in} is also shown above each panel.

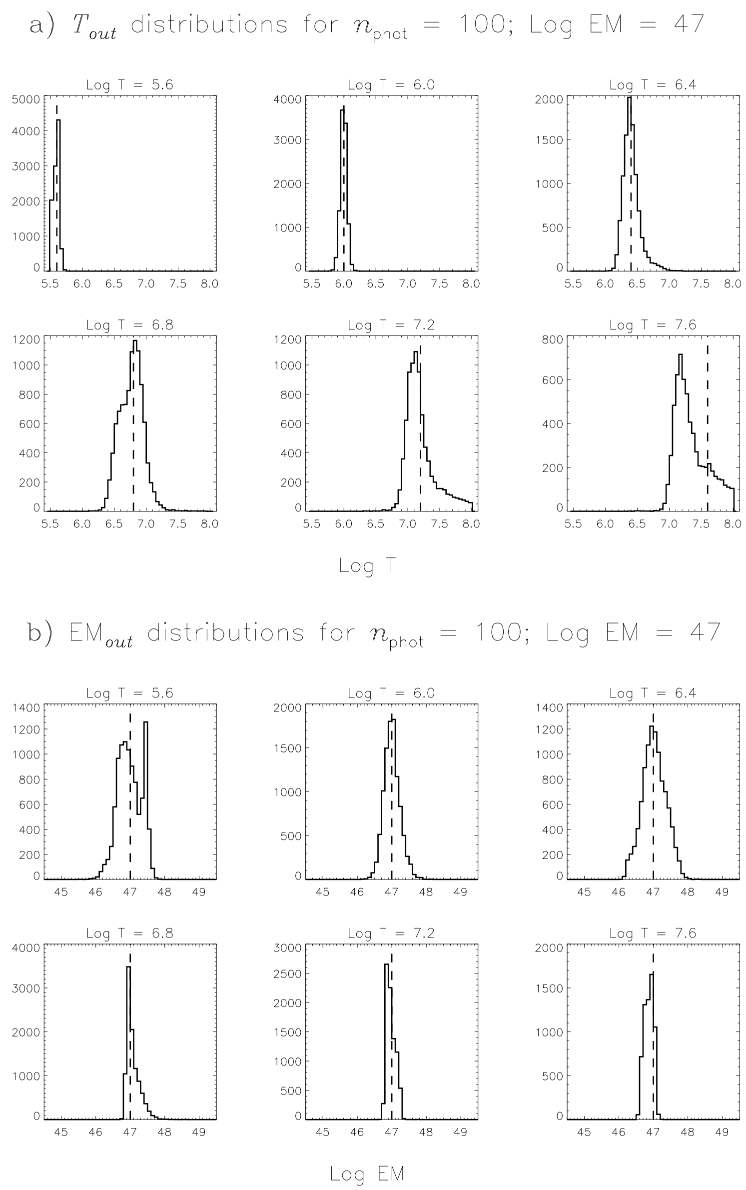

Fig. 3.— As in Fig. 2, for $n_{\rm phot} = 100$ in each SXT band.

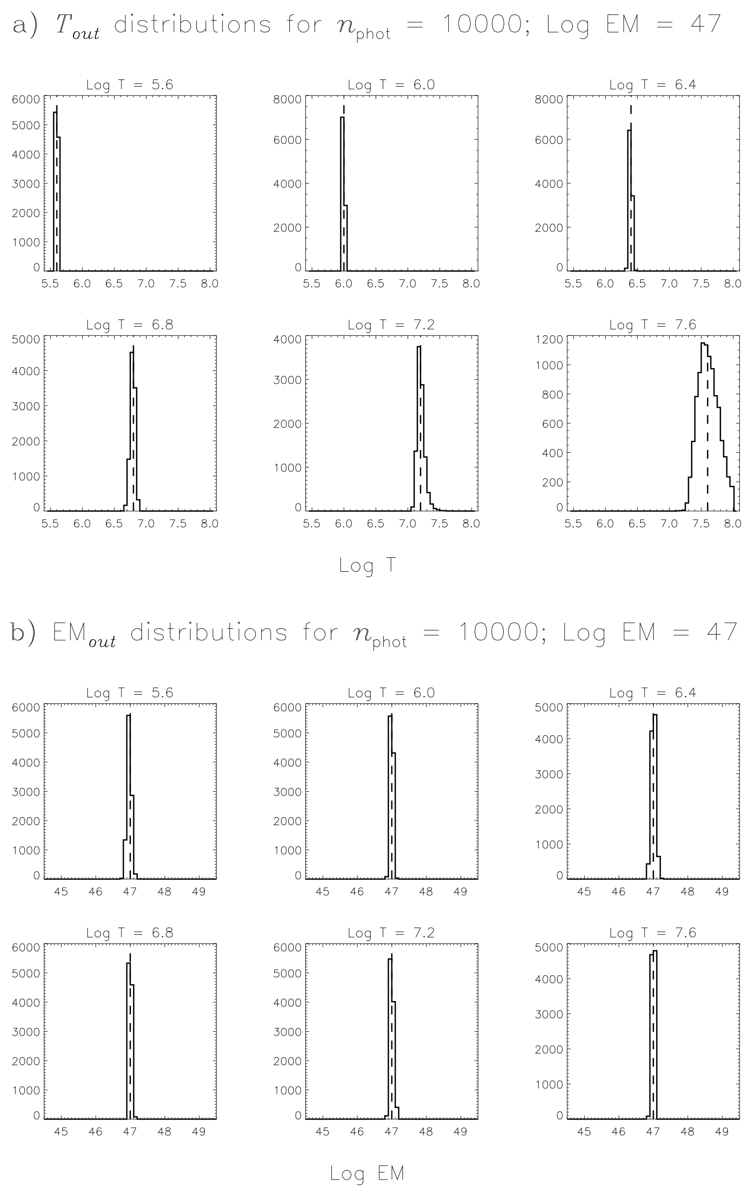

Fig. 4.— As in Fig. 2, for $n_{\rm phot} = 10^4$ in each SXT band.

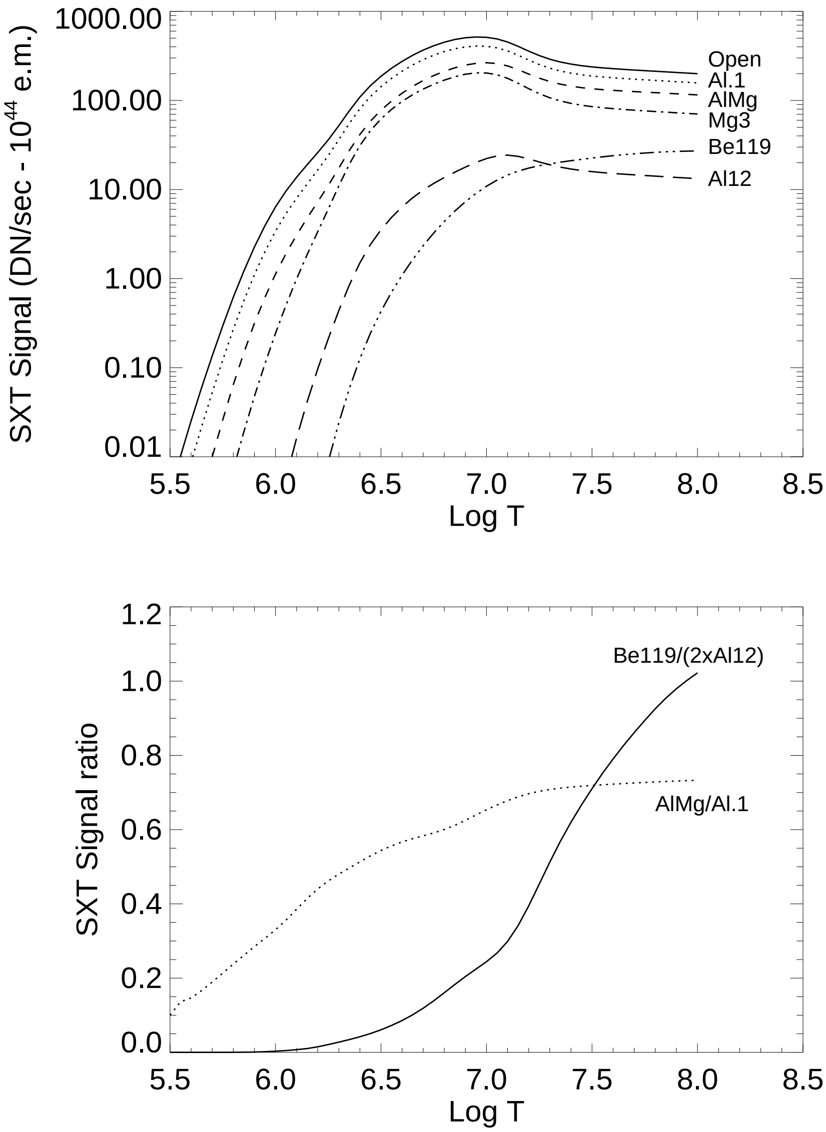

Fig. 5.— Top: Total signal vs. log T for the various bands of Yohkoh/SXT, derived with the nominal instrument spectral response and the MEKAL spectral model; Open configuration (Open), Al 1265 Å (Al.1), Al/Mg/Mn (AlMg), Mg 2.52 μm (Mg3), Al 11.6 μm (Al12), Be 119 μm (Be119). Bottom: ratios of the above SXT response functions, for the temperature determination. To be compared with the analogous figure in the *Yohkoh Analysis Guide* (Morrison 1994) which are the updated version of the figures in Tsuneta et al. (1991).

With $n_{\rm phot} = 100$, the error in the temperature is, at worst, within 40%, mostly 20% from the input value (at the 68% confidence level) for temperatures below 10^7 K, but the emission measure still has very large uncertainties for any temperature (mostly between 40% and 60% from the input value). At higher count statistics, in general, the temperature is affected by large uncertainties only for $T > 10^7$ K.

The median values and the 68% confidence range computed for each T_{out} and EM_{out} distribution provide us with the errors in the temperature and emission measure determination. As shown in Fig. 6, there are both random statistical errors and systematic shifts of the median data values with respect to the input ones (e.g. the temperatures $> 10^7$ K for $n_{\rm phot} = 10$). In Fig. 7 we report the fractional errors derived from the simulations (diamonds) as the sum in quadrature of the statistical and systematic errors, the former being the 68% confidence range and the latter being evaluated as the difference between the median and the nominal values. In the figure, we compare such a fractional errors with those derived analytically (crosses in the figure) according to the SYAS (Klimchuk and Gary 1995). The errors derived with the two approaches are in good accordance at high count statistics ($n_{\rm phot} \geq 1000$), while the errors derived analytically can be overestimated at low count statistics ($n_{\rm phot} \leq 100$).

To visualize more directly the implications of our simulations, we check how they reproduce the "seed" emission measure distribution (see Eq. 5) for the various photon count statistics. We divide the temperature range into 30 bins and sum the emission measure of all the realizations whose resulting temperature falls in the temperature bin. As discussed also in Paper II, we choose bins constant in $\log T$, for a good temperature discrimination.

Fig. 8 shows the resulting $\mathrm{EM}_{out}(T_{out})$, divided by the input $\mathrm{EM}_{in}(T_{in})$. For the lowest count statistics ($n_{\rm phot} = 10$), the normalized $\mathrm{EM}(T)$ distribution is very different from the input constant distribution and it looks like a power law with negative index: there is a large excess of emission measure for $T < 3 \times 10^6$ K and a depletion of EM for $T > 10^7$ K. The small bump at $T \sim 10^7$ K is not statistically significant as it is apparent considering the statistical uncertainties shown in Fig. 6. Fig. 6 also shows that very large statistical uncertainties shown in affect these results. For $n_{\rm phot} = 100$, the EM excess below $T = 10^6$ K is considerably reduced and at $T \sim 2 \times 10^6$ K the emission measure is slightly overestimated by a factor ~ 2. The results of the simulations approach the input distribution as the signal to noise ratio increases (i.e. for increasing $n_{\rm phot}$).

As shown by the results above, at low temperatures the statistical errors on $\mathrm{EM}(T)$ are very large; this is mostly due to the steepness of the SXT signal vs. temperature: even a moderate error of the plasma temperature may lead to a large error in the emission measure by up to two orders of magnitude. Therefore, such an effect and the large temperature errors at $T < 10^6$ K, may lead to large errors on the emission measure for $T < 10^6$ K, both in individual pixels and in the emission measure distribution of the whole corona, our task. In the latter case, we will show, the resulting $\mathrm{EM}(T)$ can be largely inaccurate.

On the other hand, for $\log T(\mathrm{K}) > 7$ the SXT signal vs. temperature is rather flat and an

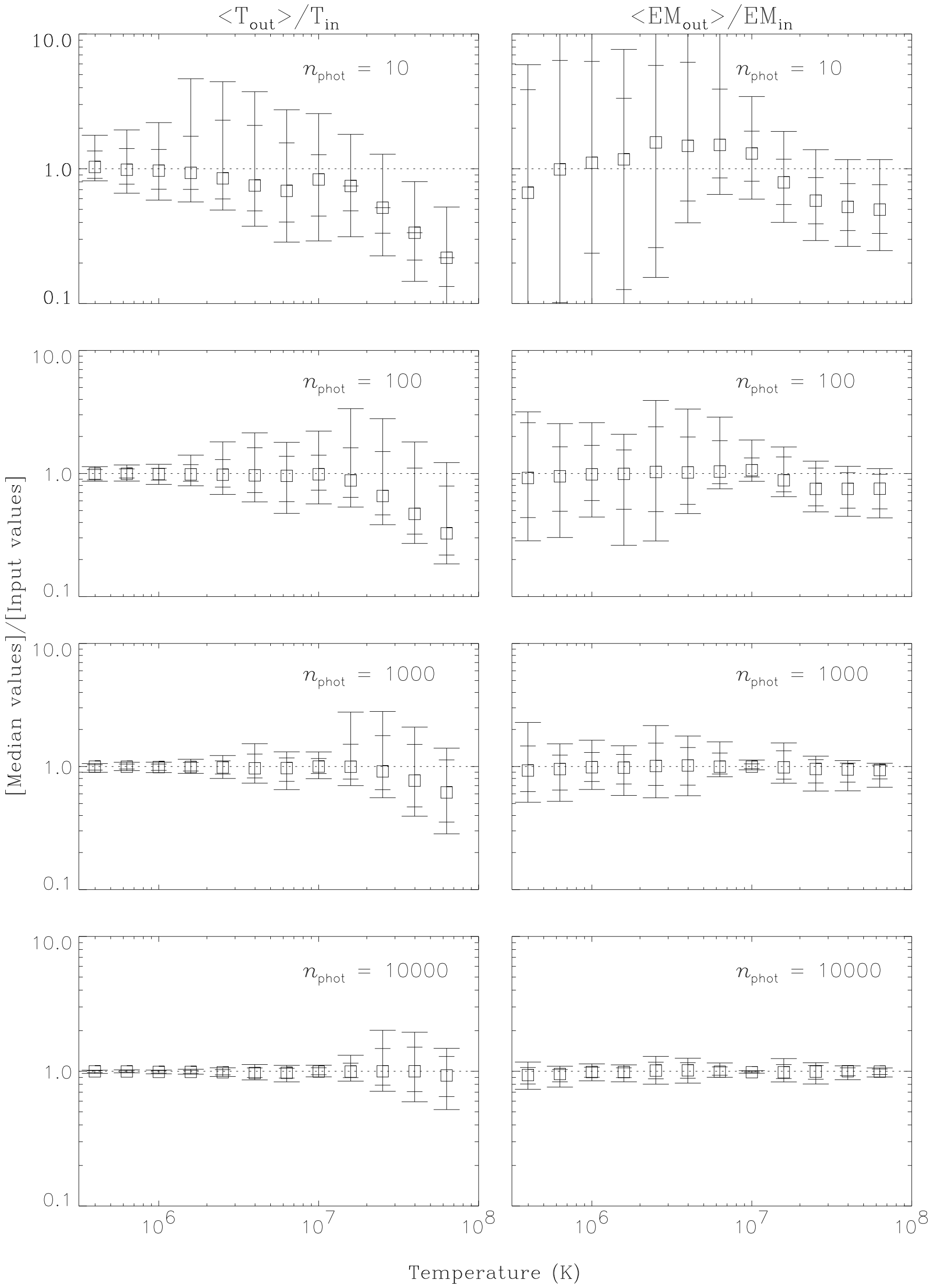

Fig. 6.— Median values (squares) divided by the input values, of the temperature (left panels) and of the emission measure (right panels) vs. temperature, along with their 68% and 90% confidence ranges marked by the horizontal lines above and below the square. The values of $n_{\rm phot}$ are reported in each panel.

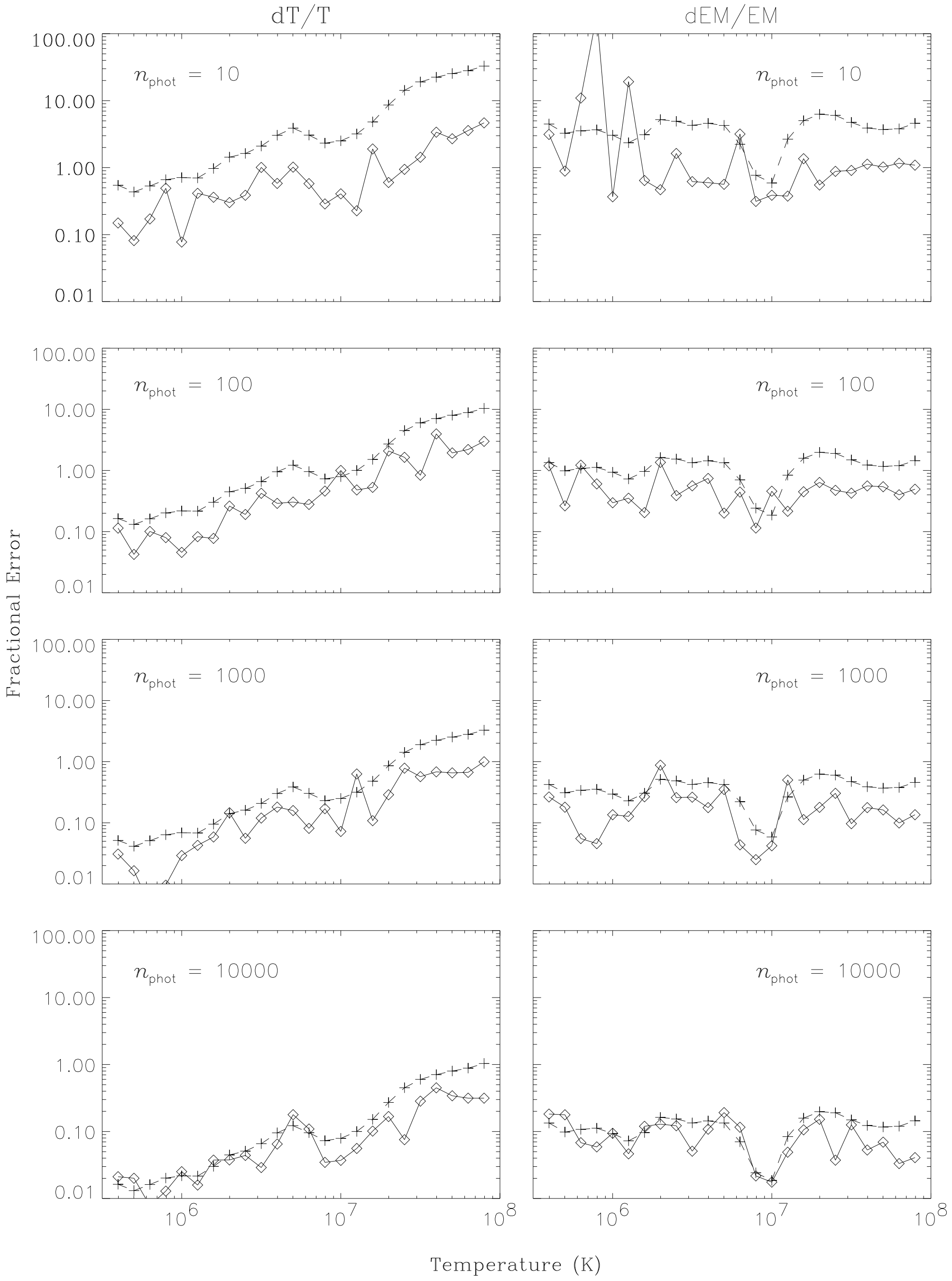

Fig. 7.— Fractional errors in temperature (left panels) and emission measure (right panels) vs. temperature derived from the simulations (diamonds) and from error analysis (crosses). The values of $n_{\rm phot}$ are reported in each panel.

underestimate in T_{out} (also a factor 10 in the case of $\log T_{in}(\mathrm{K}) \sim 8$) leads to a small underestimate in EM_{out}, not larger than a factor two in these bands, typically not used for flares. In any case, the Sun's EM above 10^7 K is so low, in absence of flares, as to make any effect at such high temperatures irrelevant.

3. Determination of EM(T) of the whole Sun

In this section we apply the insight acquired with the data simulations to analyze and to interpret real SXT data, and to derive the EM(T) of the whole solar corona.

As mentioned above, the very large dynamic range of the coronal brightness cannot be covered by the response of the CCD with only one exposure. In fact, saturated and/or underexposed regions may be present, often simultaneously, in each image. Therefore our first step is to consider the longest exposure images in a sequence; it yields the highest signal on the faintest coronal structures. We exclude the saturated pixels of the image from the analysis and we take them from a shorter exposure of the same sequence. We repeat this procedure going from the longest to the shortest exposure of the sequence and combining the pixels at the optimal signal to noise ratio in the image.

As a specific example we present an SXT observing sequence during the maximum of the solar cycle, namely January 6, 1992 (see table 1). A composite image of the Sun generated from the Al.1 filter sequence is shown in Fig. 9. This is a case of very large dynamic range of brightness, from active region cores to coronal holes. Two pairs of exposures are available close in time, i.e. within approximately eight minutes, and taken with the Al.1 and AlMg filters, each pair with a different exposure time (reported in table 1): the short exposure time images contain good data from the active region cores, the long exposure time images from the other regions.

The data are preprocessed for analysis according to the SYAS: we perform standard

Table 1. X–ray Yohkoh/SXT observations selected to derive the EM(T) distribution of the full solar disk.

N.	Date	Time	Filter	Exp. time (ms)
1	6–Jan–92	21:27:48	Al.1	78.6762
2	6–Jan–92	21:29:56	AlMg	78.0587
3	6–Jan–92	21:32:04	Al.1	2689.45
4	6–Jan–92	21:34:12	AlMg	2689.45

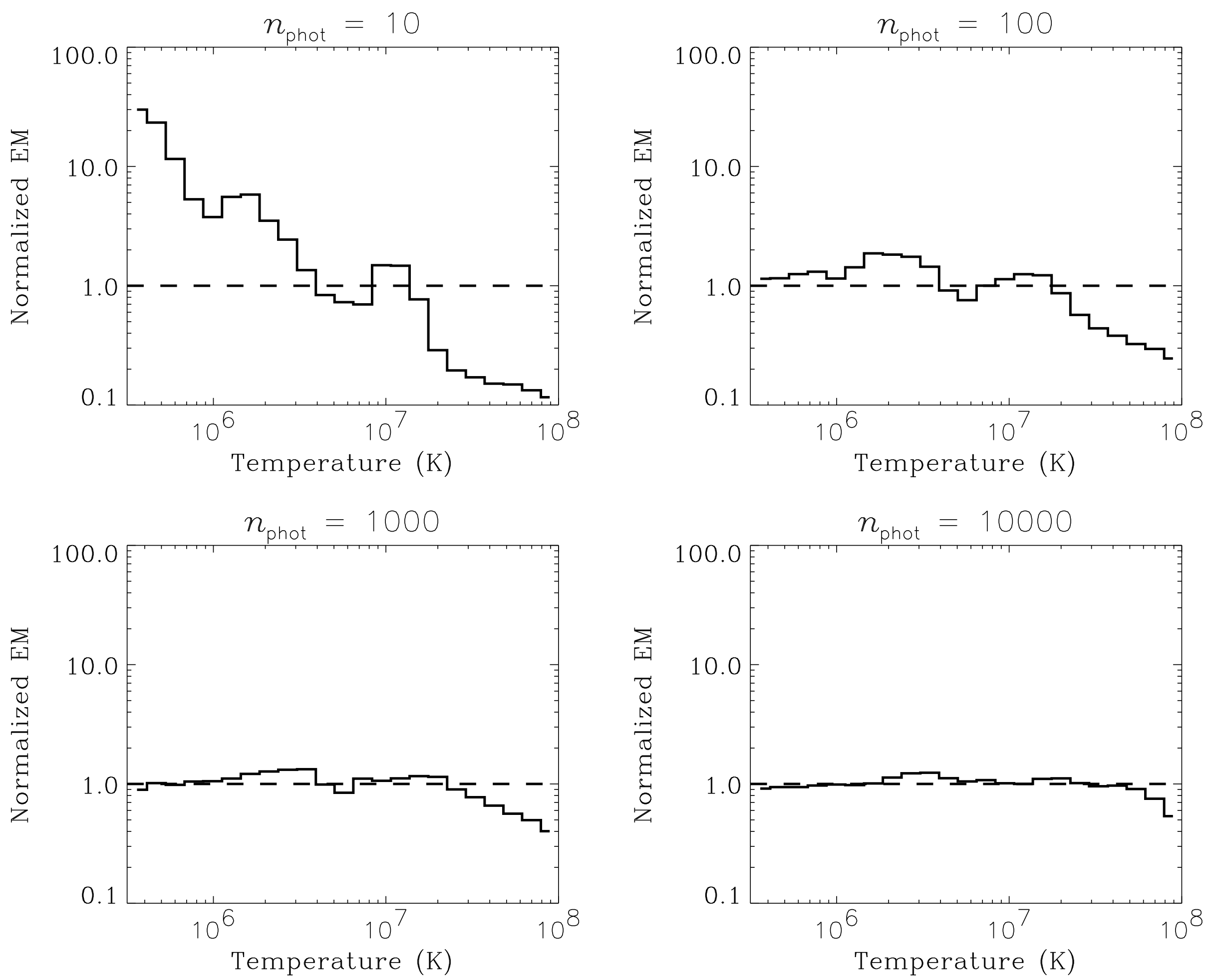

Fig. 8.— EM(T) distributions derived from the SXT data simulations (solid lines) and divided by the input $\mathrm{EM}_{in}(T_{in})$ (see Eq. 5). The dashed lines correspond to the expected result if the effects of the observations and the data analysis are zero. Each panel corresponds to different values of the total photon number $n_{\rm phot}$ in the pixel, as shown above each panel.

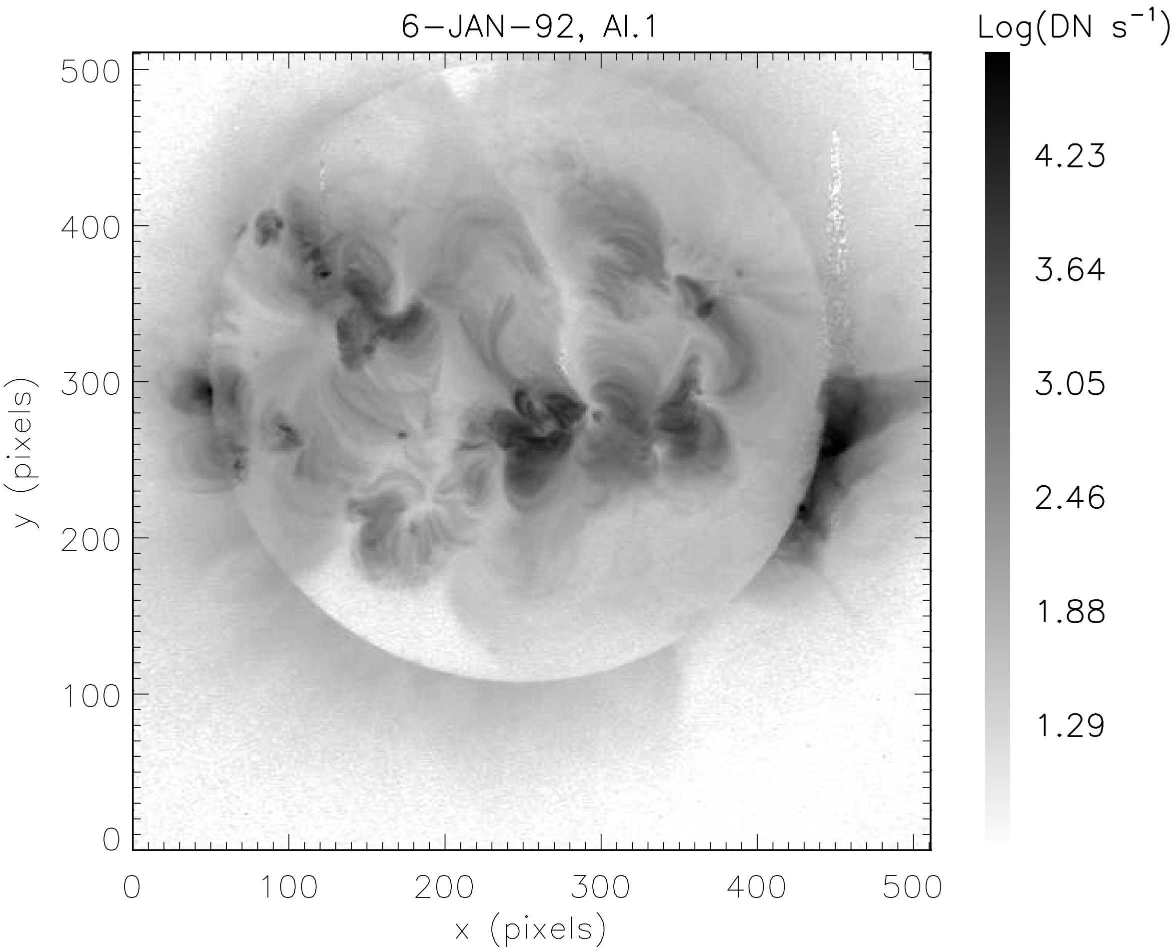

Fig. 9.— Full–Sun X–ray image of January 6, 1992 obtained by Yohkoh/SXT with the thin aluminum filter (Al.1). This image is composed of parts of two images of different exposure times (images 1 and 3 listed in table 1) in order to cover a large dynamic range. The signal in various parts is properly rescaled with the exposure time.

corrections to the data (data decompression, dark current subtraction, pin–hole visible stray light subtraction), align the images, remove the spikes, apply the vignetting correction. From the temperature and emission measure values obtained with SYAS, in each pixel we derive the folded spectrum from Eqs. 1 and 2 and then we compute the total photon counts of the focal plane (see Eqs. 1 and 2).

We then classify the SXT pixels as a function of their photon counts into four ranges of count statistics, in such a way that the results can be compared with those obtained for the four count statistics considered in our simulations (see section 2.2), albeit here we deal with range of values rather than with fixed values. In Fig. 10, we mark in gray the pixels with a photon count in the range shown above each panel; the solid contours mark the regions saturated in the long exposure time images.

For the sequence of images considered, the regions external to the solar disk, and the large coronal hole around the south pole, in the images with long exposure, yield $n_{\rm phot} \leq 10$. Also, pixel of the regions saturated in the long exposure time images, yield $n_{\rm phot} \leq 10$ in the short exposure time image. Part of the solar disk is taken from the long exposure time images and correspond to pixels with $10 < n_{\rm phot} \leq 100$. Also some regions of intermediate brightness, saturated in the images with long exposure time and underexposed in those with short exposure time, correspond to pixels with $10 < n_{\rm phot} \leq 100$. The regions of intermediate brightness taken from the images with long exposure time and the cores of the active regions taken from the images with short exposure time have pixels with $n_{\rm phot} > 100$. The fact that all the pixels with $n_{\rm phot} \leq 10$ should have, nonetheless, a very low signal (or not a significant one) depends on the time exposure selected for the image and therefore particular care should be taken when generalizing the above statements. However having chosen a sequence with typical exposure times gives a very good insight on what to expect in other sequences.

Having derived the temperature and the emission measure for each pixel[4], we then derive the EM(T) distributions, shown in Fig. 11, with the same temperature binning as the simulations in Fig. 8. Since the fractional errors derived analytically in the SYAS are in good accordance with those derived from the simulations (see Fig. 7), we adopted the former in the derivation of the error bars shown in Fig. 11. The EM(T) distribution from the pixels with $0 < n_{\rm phot} \leq 10$ is a very steep power law, reminiscent of the simulations with $n_{\rm phot} = 10$ and indicative of significant errors. Furthermore, the large total emission measure inferred from the pixels with $T < 10^6$ K is quite unrealistic and in disagreement with the findings of Brosius et al. (1996). The above simulations, considerations, and the fact that most of these pixels are located very far in the faint outer corona (see Fig. 10), confirm that these data should be discarded. In the determination of the EM(T) distribution of the whole solar corona our choice is therefore to reject all pixels with $n_{\rm phot} \leq 10$.

[4]As for the simulations, we have consistently used the up–to–date MEKAL spectral code (Kaastra 1992; Mewe et al. 1995) to produce the calibration curves to derive temperature and emission measure instead of the theoretical X–ray spectra of Mewe et al. (1985) and Mewe, Lemen, & van den Oord (1986) commonly used in the SYAS.

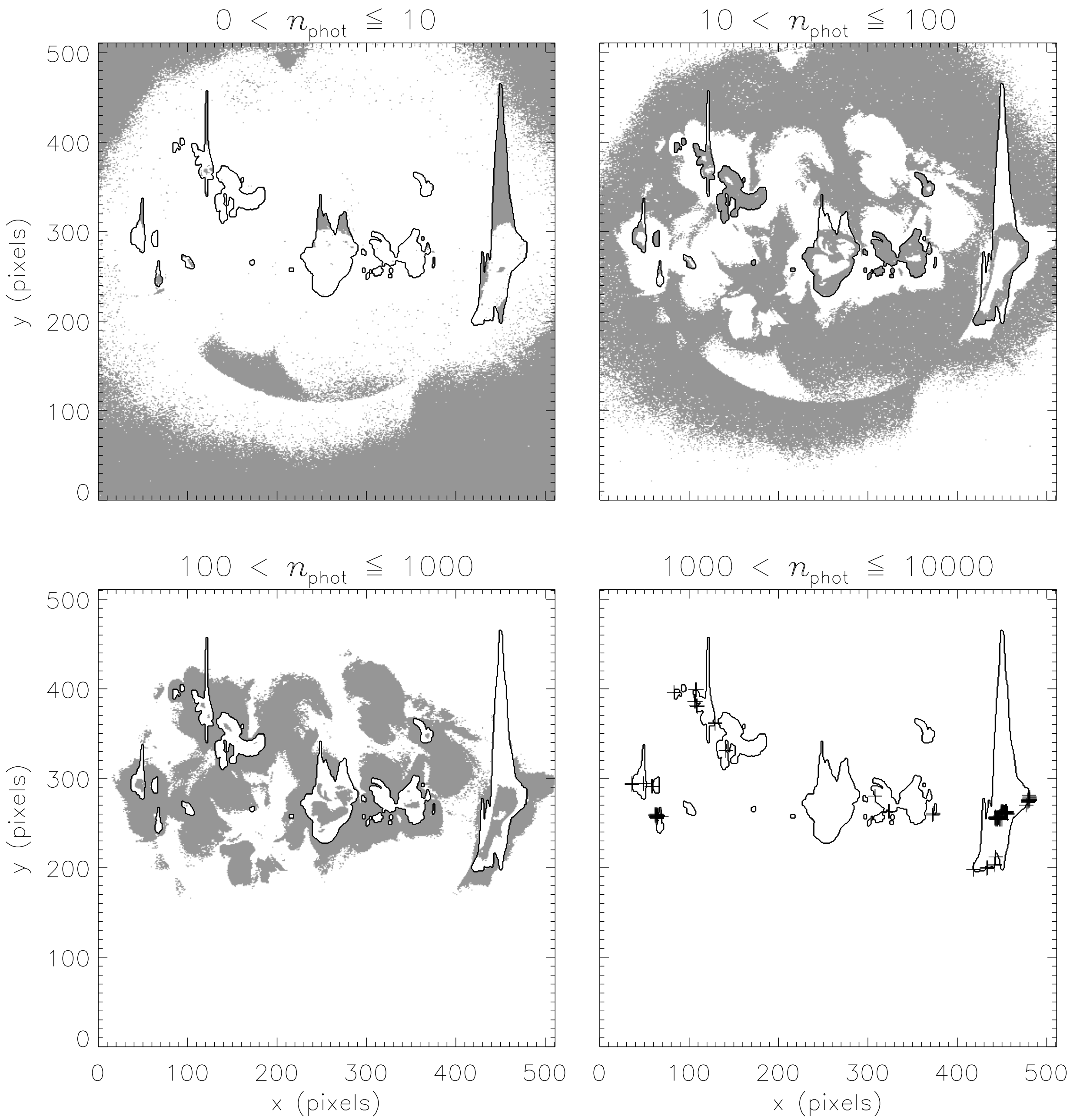

Fig. 10.— The four panels refer to the solar image of Fig. 9. Each panel shows in gray the pixels with n_{phot} in a selected range (reported above each panel): $0-10$ (*upper left* – 79699 pixels); $11-100$ (*upper right* – 132924 pixels); $101-1000$ (*lower left* – 49419 pixels). The few pixels (102) with more than 10^3 photons are, instead, marked with crosses for better visibility. The solid contours bound the regions saturated in the long exposure images and taken from the images with shorter exposure time. Note that due to strong saturation, the bright images were affected by the CCD blooming to the North.

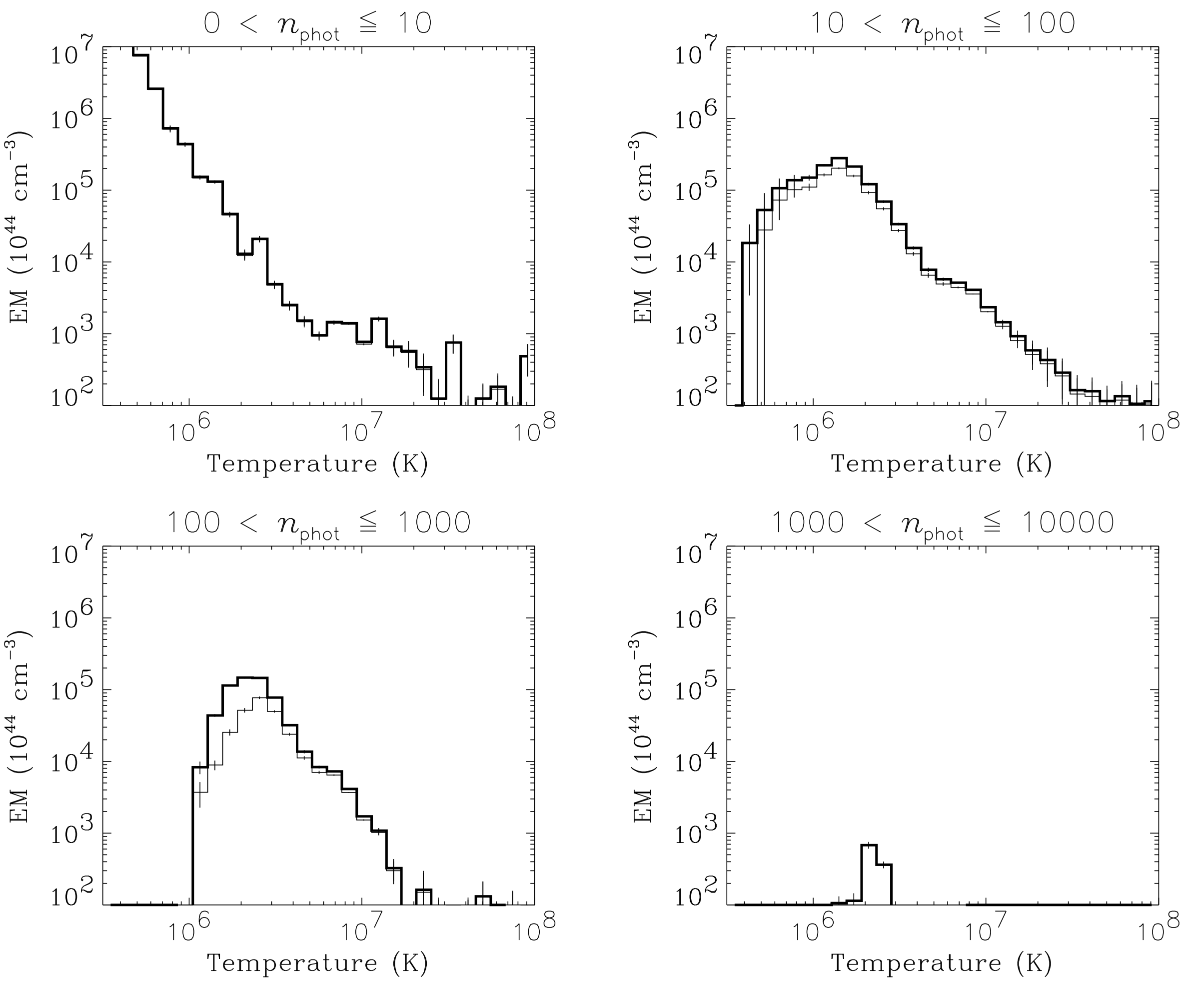

Fig. 11.— EM(T) distributions of the whole solar corona on January 6, 1992, derived from pixels with n_{phot} within the selected ranges (thick lines). The thin lines show the contribution to EM(T) due to the pixels from the images with short exposure time. Each panel corresponds to the same range of n_{phot} as in Fig. 10. We also show the statistical errors (vertical lines).

The panels with higher photon counts show several interesting features: the distribution for $10 \leq n_{\rm phot} \leq 100$ is characterized by a moderate steep ascent up to 2×10^6 K and a rather steep descent toward higher temperatures. The distribution for $100 \leq n_{\rm phot} \leq 10^3$ is bell shaped with a steep ascent of EM(T) up to $T \approx 2 \times 10^6$ K and a steep descent for $T > 2 \times 10^6$ K. The few pixels with $n_{\rm phot} > 10^3$ are grouped around 2×10^6 K.

Fig. 12 shows the complete EM(T) distribution derived from the SXT data collected on January 6, 1992, with the screening criterion described above (thick line). The distribution is characterized by a maximum at $T \sim 2 \times 10^6$ K and shows a $T^{3/2}$ rise at transition region temperatures (dashed line), a characteristics in agreement with other studies of the solar atmosphere mostly done in the UV band (see also Jordan 1980, Brosius et al. 1996, Landi & Landini 1997). In the same figure we show the EM(T) distribution that we would obtain including all the pixels in our analysis (thin line). Whereas the two distributions are quite similar for $T > 2 \times 10^6$ K, the EM(T) derived without a screening criterion shows a huge excess of emission measure for $T < 2 \times 10^6$ K, in clear disagreement with EUV observations (Brosius et al. 1996).

4. Summary and discussion

In this paper Yohkoh/SXT data are analyzed and interpreted with the aid of detailed simulations to determine reliably the emission measure distribution vs. temperature of the whole solar corona. This distribution is our basis to study the Sun as an X–ray star; in Paper II, we describe the whole method to derive the stellar–like spectra of the Sun from the Yohkoh/SXT data. Here we have concentrated our attention on the simulations, the criteria adopted and the derivation of the EM(T).

The simulations cover the $10^{5.5} - 10^8$ K temperature range and consider from 10 to 10^4 photon counts, extensively covering the possible conditions in a SXT image pixel. The simulations shown here allow us to study the influence of instrumental and statistical effects on the data, including high and low brightness regions, to correct for them and therefore to use simultaneously all the information present in the emitting corona, in order to derive the EM(T) of the whole Sun. This would be a relatively easy feat, if the exposure times in each images sequence were such to cover exhaustively the entire dynamic range of the corona brightness, but for most sequences this is not the case and the task, as we have discussed, is more complex.

Our analysis, apart from showing how to make best uses of the SXT observations for our tasks, also suggests possible improvements for future observations with respect to the usual Yohkoh/SXT full–disk image sequences, typically with only two exposure times (e.g. 78 ms and 2668 ms in the Al.1 and AlMg filters): in most of the sequences, typically the coronal regions surrounding the active region cores are either saturated, in the long exposure time images, or too faint in the short exposure images. We suggest to take additional images with a range of intermediate exposure times more closely spaced and appropriate to span the entire brightness

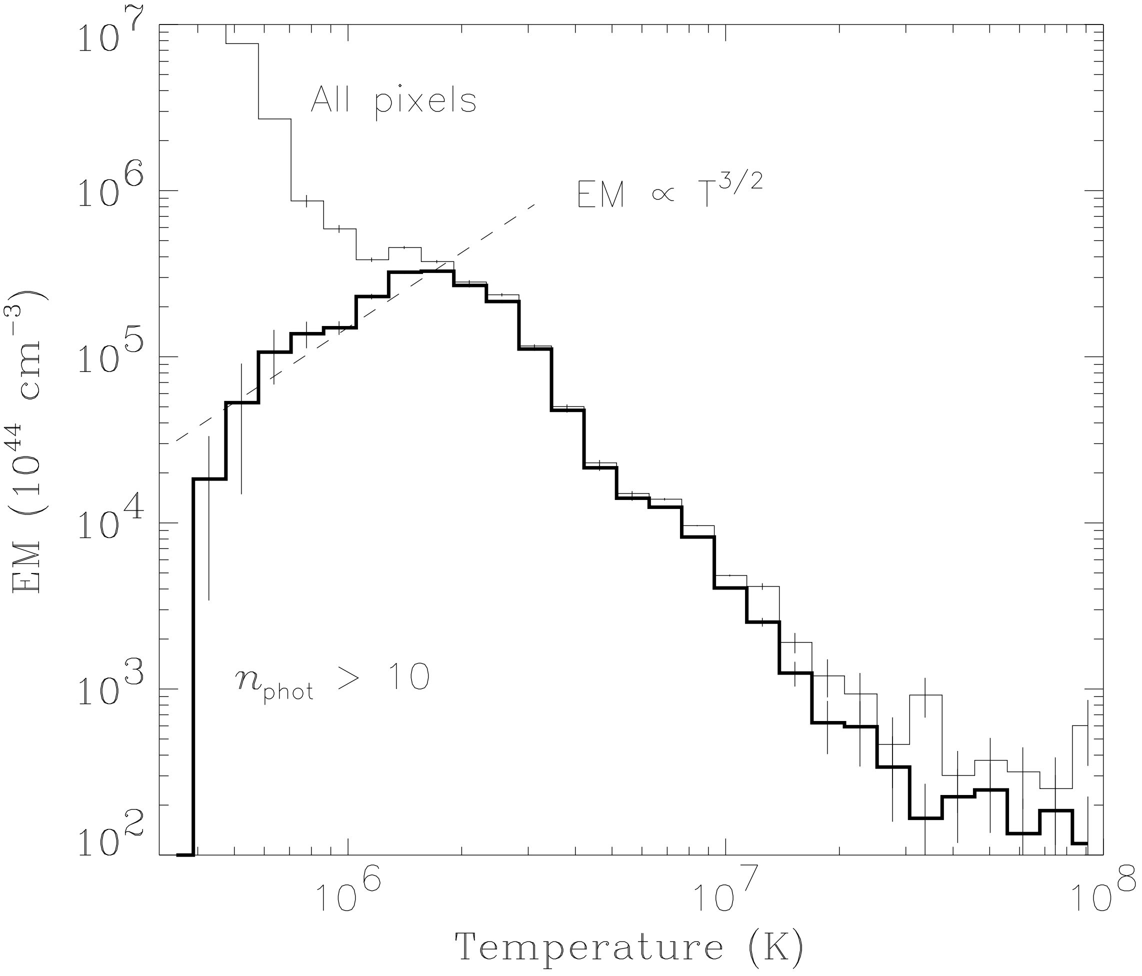

Fig. 12.— Emission measure distribution vs. temperature of the solar corona, considering all the pixels (thin line) and selecting only the pixels with good signal to noise, i.e. $n_{\rm phot} \geq 10$ (thick line). The dashed line marks the slope $T^{3/2}$ of the EM(T) distribution.

dynamic range of the corona.

Another point of interest in the context of solar–stellar connection studies, although not as important as the one just mentioned, is to study the possible presence of plasma at $T \geq 10^7$ K outside flares. The relevant findings are of interest in view of observations of very active stars showing large emission measure values (EM $\sim 10^{52}$ cm^{-3}) around or above $\sim 10^7$ K without evident flares (Schmitt et al. 1990, Antunes, Nagase, & White 1994, Drake et al. 1994, White et al. 1994, Singh, Drake, & White 1995, Kaastra et al. 1996, Singh, White, & Drake 1996, Güdel 1997, Güdel, Guinan, & Skinner 1997). Observations of the full disk of the Sun with the hardest SXT filters (Al12 and Be119 filters) and with long exposure times (e.g. ~ 2.0 s and ~ 3.2 s using respectively the Al12 and Be119 filters to detect at least 100 photons in each of the two bands emitted by a plasma with $T = 2 \times 10^7$ K and EM $= 10^{45}$ cm^{-3}) should yield enough signal to noise ratio to get appropriate information on $T > 10^7$ K plasma.

The present study shows that the emission measure, as determined from SXT data, may be subject to large errors for $T < 10^6$ K, as shown in Fig. 6. Indeed, because of the very steep SXT response vs. temperature in that range, a small error in temperature may lead to a large error on emission measure at low signal to noise ratio. However we recover the information in this crucial range of temperature by accepting only the pixels with more than 10 photons in each of the two bands needed for the T determination. The pixels with $n_{\rm phot} < 10$ have such a large error to make any T and EM determination worthless. In particular, we have shown that an EM(T) distribution derived from low–count data with $n_{\rm phot} < 10$ with a steep negative slope like that shown in Fig. 11 is indicative of significant errors. The EM indetermination at $T < 10^6$ K is significantly reduced by rejecting pixels with $n_{\rm phot} \leq 10$.

We have applied our method to a real observation made by Yohkoh/SXT on January 6 1992, i.e. during the period of maximum activity of the Sun, which shows a very large dynamic range of brightness and, therefore, is a challenging case. We obtain an EM(T) distribution of the whole solar corona, for $T \leq 10^6$ K consistent with previous results obtained mostly with UV instruments – see, for example, the analysis of Brosius et al. (1996) based on the SERTS data and that by Landi & Landini (1997) based on SOHO and, more in general, with the established fact that the solar corona EM rises as $\sim T^{3/2}$ or T^2 up to $\sim 10^6$ K (Jordan 1980).

Watanabe et al. (1995), studying active regions, used temperature bins uniform in a linear temperature scale and, more important, the pixels in each image were grouped, thus forming macro–pixels (8×8) to increase significantly the signal to noise ratio. We have found that grouping pixels is tolerable for 2×2 macro–pixels but may distort the emission measure curve by averaging any temperature structure, even at high signal to noise ratio values. Watanabe et al. (1995), furthermore, concentrate on plasma above $\sim 10^6$ K, as many other authors do with Yohkoh/SXT data. Our interest is however for the complete nominal temperature range, including that below 10^6 K, where still significant solar coronal emission measure is and many non–solar instruments (e.g. Rosat and XMM) are sensitive.

With the set of simulations and the relevant analysis here presented, we have studied the errors arising in the temperature and emission measure determination from Yohkoh/SXT full disk images. We also presented a method to derive a reliable emission measure vs. temperature distribution of the whole corona, a fundamental step for our project dedicated to use the solar corona as a template for other stellar coronae and to study the temperature distribution in the solar corona. The present results and the whole project itself may also be of importance in the perspective of other Yohkoh/SXT–like instruments such as the Solar X–Ray Imager[5].

We are grateful to the anonymous referee and to R. Rosner for useful criticisms and suggestions which allowed us to improve significantly the paper. This work was supported in part by Agenzia Spaziale Italiana and by Ministero della Università e della Ricerca Scientifica e Tecnologica.

[5]The Solar X–Ray Imager (SXI) is being built to fly on the Geosynchronous Operational Environmental Satellite (GOES) for the NOAA (National Oceanic and Atmospheric Administration) Space Environment Center.

REFERENCES

Acton, L. 1997, in Observational Plasma Astrophysics: Five Years of Yohkoh and beyond, Proc. of the Yohkoh 5th Anniversary Symp., Yoyogi, Tokyo, Japan, November 1996

Antunes, A., Nagase, F., White, N. E. 1994, ApJ, 436, L83

Brosius, J. W., Davila, J. M., Thomas, R. J., Monsignori–Fossi, B. C. 1996, ApJS, 106, 143

Brosius, J. W., Davila, J. M., Thomas, R. J., Saba, J. L. R., Hara, H., Monsignori–Fossi, B. C. 1997, ApJ, 477, 969

Drake, J. J., Peres, G., Orlando, S., Laming, J. M., et al. (1998), ApJ, in preparation.

Drake, S. A., Singh, K. P., White, N. E., Simon, T. 1994, ApJ, 436, L87

Gerassimenko, M., Nolte, J. 1978, Sol. Phys., 60, 299

Güdel, M. 1997, ApJ, 480, L121

Güdel, M., Guinan, E. F., Skinner, S. L. 1997, ApJ, 483, 947

Hara, H., Tsuneta, S., Lemen, J. R., Acton, L. W., McTiernan, J. M. 1992, PASJ, 44, L135

Jordan, C. 1980, A&A, 86, 355

Kaastra, J. S. 1992, An X–Ray Spectral Code for Optically Thin Plasmas, Internal SRON–Leiden Report, updated version 2.0

Kaastra, J. S., Mewe, R., Liedahl, D. A., Singh, K. P., White, N. E., Drake, S. A. 1996, A&A, 314, 547

Kano, R., Tsuneta, S. 1995, ApJ, 454, 934

Klimchuk, J. A., Gary, D. E. 1995, ApJ, 448, 925

Landi, E. and Landini, M., 1997, in "The Corona and Solar Wind near Minimum Activity", Proc. of the 5th SOHO Workshop, A. Wilson ed., ESA SP–404

Mewe, R., Gronenschild, E. H. B. M., van den Oord, G. H. J. 1985, A&AS, 62, 197

Morrison, M. 1994, "Yohkoh Analysis Guide. Volume 3: Instrument Guide"

Mewe, R., Lemen, J. R., van den Oord, G. H. J. 1986, A&AS, 63, 511

Mewe, R., Kaastra, J. S., Liedhal, D. A. 1995, Legacy 6, 16

Peres, G., Orlando, S., Reale, F., Rosner, R., & Hudson, H. 1998, ApJ, in preparation

Porter, L., & Klimchuk, J. A. 1995, ApJ, 454, 499

Press, W.H., Flannery, B.P., Teukolsky, S.A., Vetterling, W.T. 1986, "Numerical Recipes", (New York: Cambridge Univ. Press)

Schmitt, J. H. M. M., Micela, G., Sciortino, S., Vaiana, G. S., Harnden, F. R. Jr., Rosner, R. 1990, ApJ, 351, 492

Singh, K. P., Drake, S. A., White, N. E. 1995, ApJ, 445, 840

Singh, K. P., White, N. E., Drake, S. A. 1996, ApJ, 456, 766

Tsuneta, S. 1996, ApJ, 456, 840

Tsuneta, S., et al. 1991, Sol. Phys., 136, 37

Vaiana, G. S., Krieger, A., Timothy, A. 1973, Sol. Phys., 32, 81

Yoshida, T., Tsuneta, S., Golub, L., Strong, K., Ogawara, Y. 1995, PASJ, 47, L15

Yoshida, T., Tsuneta, S. 1996, ApJ, 459, 342

Watanabe, T., Hara, H., Shimizu, T., Hiei, E., Bentley, R. D., Lang, J., Phillips, K. J. H., Pike C. D., Fludra, A., Bromage, B. J. I., Mariska, J. 1995, Sol. Phys., 157, 169

White, N. E., et al. 1994, PASJ, 46, L97